

Design of a photonic crystal fiber polarization beam splitter with simple structure and ultra-wide bandwidth

Yun-Peng Wei(魏云鹏), Jin-Hui Yuan(苑金辉), Yu-Wei Qu(屈玉玮), Shi Qiu(邱石), Xian Zhou(周娴), Bin-Bin Yan(颜玢玢), Kui-Ru Wang(王葵如), Xin-Zhu Sang(桑新柱), and Chong-Xiu Yu(余重秀)
Citation: Chin. Phys. B, 2023, 32 (**10**): 104210. DOI: 10.1088/1674-1056/accd54
Journal homepage: http://cpb.iphy.ac.cn; http://iopscience.iop.org/cpb

What follows is a list of articles you may be interested in

Multi-band polarization switch based on magnetic fluid filled dual-core photonic crystal fiber

Lianzhen Zhang(张连震), Xuedian Zhang(张学典), Xiantong Yu(俞宪同), Xuejing Liu(刘学静), Jun Zhou(周军), Min Chang(常敏), Na Yang(杨娜), and Jia Du(杜嘉)
Chin. Phys. B, 2023, 32 (**2**): 024205. DOI: 10.1088/1674-1056/ac9a37

Design of a polarization splitter for an ultra-broadband dual-core photonic crystal fiber

Yongtao Li(李永涛), Jiesong Deng(邓洁松), Zhen Yang(阳圳), Hui Zou(邹辉), and Yuzhou Ma(马玉周)
Chin. Phys. B, 2022, 31 (**5**): 054215. DOI: 10.1088/1674-1056/ac3a63

Ultra-broadband polarization splitter based on graphene layer-filled dual-core photonic crystal fiber

Hui Zou(邹辉), Hui Xiong(熊慧), Yun-Shan Zhang(张云山), Yong Ma(马勇), Jia-Jin Zheng(郑加金)
Chin. Phys. B, 2017, 26 (**12**): 124216. DOI: 10.1088/1674-1056/26/12/124216

Designing of a polarization beam splitter for the wavelength of1310 nm on dual-core photonic crystal fiber with high birefringence and double-zero dispersion

Bao Ya-Jie (鲍亚杰), Li Shu-Guang (李曙光), Zhang Wan (张婉), An Guo-Wen (安国文), Fan Zhen-Kai (范振凯)
Chin. Phys. B, 2014, 23 (**10**): 104218. DOI: 10.1088/1674-1056/23/10/104218

Designing analysis of the polarization beam splitter in two communication bands based on a gold-filled dual-corephotonic crystal fiber

Fan Zhen-Kai (范振凯), Li Shu-Guang (李曙光), Fan Yu-Qiu (范玉秋), Zhang Wan (张婉), An Guo-Wen (安国文), Bao Ya-Jie (鲍亚杰)
Chin. Phys. B, 2014, 23 (**9**): 094212. DOI: 10.1088/1674-1056/23/9/094212

Design of a photonic crystal fiber polarization beam splitter with simple structure and ultra-wide bandwidth

Yun-Peng Wei(魏云鹏)[1], Jin-Hui Yuan(苑金辉)[1,2,†], Yu-Wei Qu(屈玉玮)[1], Shi Qiu(邱石)[1], Xian Zhou(周娴)[2], Bin-Bin Yan(颜玢玢)[1], Kui-Ru Wang(王葵如)[1], Xin-Zhu Sang(桑新柱)[1], and Chong-Xiu Yu(余重秀)[1]

[1] *State Key Laboratory of Information Photonics and Optical Communications, Beijing University of Posts and Telecommunications, Beijing* 100876, *China*
[2] *Research Center for Convergence Networks and Ubiquitous Services, University of Science & Technology Beijing (USTB), Beijing* 100083, *China*

(Received 8 January 2023; revised manuscript received 13 April 2023; accepted manuscript online 17 April 2023)

A novel polarization beam splitter (PBS) based on dual-core photonic crystal fiber (DC-PCF) is proposed in this work. The proposed DC-PCF PBS contains two kinds of lattices and three kinds of air holes to form the asymmetrical elliptic dual-core structure. By using the full-vector finite element method, the propagation characteristics of the proposed DC-PCF PBS are investigated. The simulation results show that the bandwidth of the proposed DC-PCF PBS can reach to 340 nm, which covers the S + C + L + U communication bands, the shortest splitting length is 1.97 mm, and the maximum extinction ratio appears near wavelength 1550 nm. Moreover, the insertion loss of the proposed DC-PCF PBS is very low. It is believed that the proposed DC-PCF PBS has important applications in the field of all-optical communication and network.

Keywords: dual-core photonic crystal fiber, polarization beam splitter, extinction ratio, bandwidth

PACS: 42.81.Gs, 42.68.Ay, 42.25.Bs, 42.81.–i **DOI:** 10.1088/1674-1056/accd54

1. Introduction

Polarization beam splitter (PBS), as one of the essential components, can be used as the polarization division multiplexer, optical filter, optical splitter, *etc*. in optical communication and sensing systems.[1–5] It is mainly used to separate the light beams in the orthogonal polarization directions.[6–9] Over the past two decades, photonic crystal fiber (PCFs) have received great attention due to their unique optical characteristics.[10–14] In recent years, some researches have concentrated on the PBSs based on the dual-core PCFs (DC-PCFs).[15,16] In 2019, Chu *et al.* designed a DC-PCF PBS fabricated with $Ge_{20}Sb_{15}Se_{65}$ glass, where the splitting length of 63 μm and working bandwidth of 80 nm are achieved.[17] In 2021, Zhang *et al.* proposed a DC-PCF PBS based on $Ge_{10}As_{22}Se_{68}$ glass, and their simulation results showed that the working bandwidth and splitting length are 60 nm and 636 μm, respectively.[18] In the same year, Ren *et al.* demonstrated a silica DC-PCF PBS, with the working bandwidth of 48 nm and the splitting length of 254 μm.[19] In 2022, Zhang investigated a compact gallium sulfide DC-PCF PBS, whose working bandwidth is 170 nm and splitting length is 277.1 μm.[20]

Generally speaking, the performances of the DC-PCF PBS can be improved by selectively filling different functional materials (such as gold, silver, and liquid crystal) into the cladding air holes.[21] In 2021, Zhang *et al*. designed a gold wire-filled DC-PCF PBS with the three kinds of air holes, where the working bandwidth is 120 nm and the splitting length is 249.12 μm.[22] In 2022, Qu *et al.* proposed a gold wire-filled X-shaped DC-PCF PBS based on the $Ge_{20}Sb_{15}Se_{65}$ glass, where the working bandwidth is 358 nm and the splitting length is 230 μm.[23] However, it brings new challenges to the preparation to fill the functional materials into the air holes.[24]

Proposed in this work is a DC-PCF PBS with simple structure and ultra-wide bandwidth. With the full-vector finite element method (FV-FEM), the influences of the structure parameters of the DC-PCF PBS on the coupling length (CL) and coupling length ratio (CLR) are investigated. The simulation results show that the proposed DC-PCF PBS has a large bandwidth of 340 nm, covering the S + C + L + U communication bands, a splitting length of 1.97 mm, and an extinction ratio (ER) of 59.08 dB at wavelength 1.55 μm.

2. Design of DC-PCF PBS and theory

Figure 1 shows the cross-sectional structure of the proposed DC-PCF PBS. The simple structure contains the rectangular and hexagonal lattices and three kinds of air holes in the cladding region. The asymmetrical elliptic cores A and B are formed by separately removing the two air holes in the X direction or Y direction. The ten largest air holes with the diameter d_1 lie in the Y direction of the core A and ±45° angle direction of the core B, five larger air holes with the diameter d_2 lie in the X direction of the core A and Y direction of the

†Corresponding author. E-mail: yuanjinhui81@163.com

© 2023 Chinese Physical Society and IOP Publishing Ltd

core B, and other air holes with the diameter d_3 are distributed in the outer region of the cladding. The hole-to-hole pitch of the rectangular lattices is Λ, so the hole-to-hole pitch of the Y direction and the diagonal direction in the hexagonal lattice are Λ and $\sqrt{5}\Lambda$ separately. In the simulation, the complete grid contains 57630 domain elements, and the grid size of the perfectly matched layer (PML), silica, and air holes are all set to $\lambda/6$. The scattering boundary condition is set at the edge of the structure, and the PML is set at the periphery of the structure. The thickness of the PML is Λ, and its refractive index is set to 0.03, which is higher than the silica material's.[25] The PML and scattering boundary condition can ensure that no reflection occurs at the boundary when the light beam enters the outer space. The thickness of the PML can affect the calculation accuracy and time.[25]

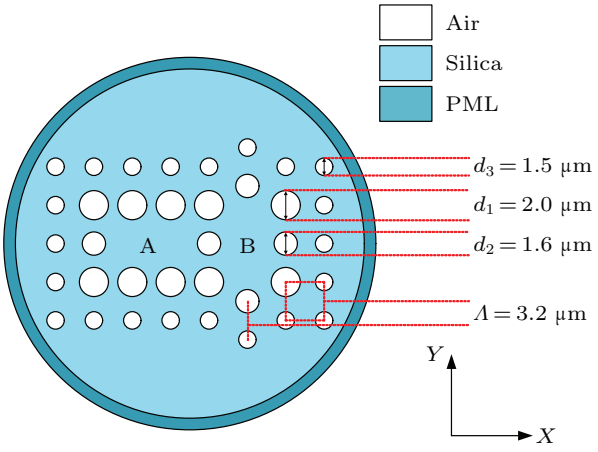


Fig. 1. Cross-sectional structure of the proposed DC-PCF PBS.

We use the following dispersion equation to describe the refractive index of silica[26]

$$n_{\text{silica}}(\lambda) = \sqrt{1 + \frac{A_1\lambda^2}{\lambda^2 - B_1^2} + \frac{A_2\lambda^2}{\lambda^2 - B_2^2} + \frac{A_3\lambda^2}{\lambda^2 - B_3^2}}, \tag{1}$$

where $A_1 = 0.6961663$, $A_2 = 0.4079426$, $A_3 = 0.8974794$, $B_1 = 0.0684043$ μm^2, $B_2 = 0.1162414$ μm^2, and $B_3 = 9.896161$ μm^2. The related coefficients are determined by the specific material (fused silica) and temperature (25 °C).[27]

According to the dual-core coupled mode theory, there should exist four supermodes when the incident light enters one of the cores A and B. That is, the X-polarized (X-pol) odd mode, X-pol even mode, Y-polarized (Y-pol) odd mode, and Y-pol even mode. Because of the difference in propagation constant between the X-pol and Y-pol odd and even modes, the light energy will transfer periodically between the two cores.[28] To describe the propagation and coupling characteristics of the X-pol light and Y-pol light in the proposed DC-PCF PBS, the coupling length (CL) of each polarized light can be calculated from the following formula[29]

$$\text{CL}_{X,Y} = \frac{\lambda}{2|n_{X,Y}^{\text{even}} - n_{X,Y}^{\text{odd}}|}, \tag{2}$$

where $\text{CL}_{X,Y}$ represent the CL of the X-pol light or Y-pol light, and n_X^{even}, n_Y^{even}, n_X^{odd}, and n_Y^{odd} denote the effective refractive indices of the considered four supermodes. Then, the CLR can be calculated by using the CL_X and CL_Y[30]

$$\text{CLR} = \frac{\text{CL}_Y}{\text{CL}_X}. \tag{3}$$

According to the working principle, when the mixed polarized light enters the core A or core B, it will be completely split into the X-pol light and Y-pol light at a specific splitting length.[31] In the following, the normalized output power (NOP) is used to describe the transfer of the light energy between the core A and the core B at different propagation distances:[32]

$$P_{\text{out,A}}^{X,Y} = P_{\text{in}} \cos^2\left(\frac{\pi}{2}\frac{L_{\text{P}}}{\text{CL}_{X,Y}}\right), \tag{4}$$

$$P_{\text{out,B}}^{X,Y} = P_{\text{in}} \sin^2\left(\frac{\pi}{2}\frac{L_{\text{P}}}{\text{CL}_{X,Y}}\right), \tag{5}$$

where L_{P}, P_{in}, and P_{out} represent the splitting length, the incident light power, the output light powers from the two cores, respectively. According to Eqs. (4) and (5), the variation of the NOP with splitting length at a specific wavelength can be obtained, and the variation of the NOP with wavelength at a specific splitting length can also be obtained. The extinction ratio (ER) is defined as[33]

$$\text{ER}_{\text{A}} = 10\lg\frac{P_{\text{out,A}}^{X}}{P_{\text{out,A}}^{Y}}, \tag{6}$$

where the ER can directly evaluate the performance of the proposed DC-PCF PBS. When the ER value is larger than ±20 dB, the power of one polarized light is 100 times higher than the other one and it is enough to separate two orthogonal polarization light beams.[34] Therefore, the wavelength range in which the ER is greater than ±20 dB can be considered as the working bandwidth of the DC-PCF PBS.[35]

We also calculate the insertion loss of the DC-PCF PBS.[36] The insertion loss $\text{IL}_{X,Y}$ can be expressed as[37]

$$\text{IL}_{X,Y} = -10\lg\frac{P_{\text{out,A}}^{X,Y}}{P_{\text{in}}}. \tag{7}$$

3. Simulation results and discussion

The initial structure parameters of the proposed DC-PCF PBS are chosen as follows: $d_1 = 2.0$ μm, $d_2 = 1.6$ μm, $d_3 = 1.5$ μm, and $\Lambda = 3.2$ μm. With the FV-FEM, the effective refractive indices of the four supermodes in the wavelength range from 1.3 μm to 1.8 μm are shown in Fig. 2. Figure 2 shows that the effective refractive indices of the four supermodes drop gradually as wavelength increases, and those of the X-pol and Y-pol even modes are always higher than those

of the X-pol and Y-pol odd modes. Besides, as wavelength increases, the difference between the effective refractive indices becomes larger. The mode field distributions calculated at wavelength 1.55 μm are shown in Figs. 3(a)–3(d). It can be seen from Figs. 3(a)–3(d) that the mode field energy can be well confined in the cores A and B.

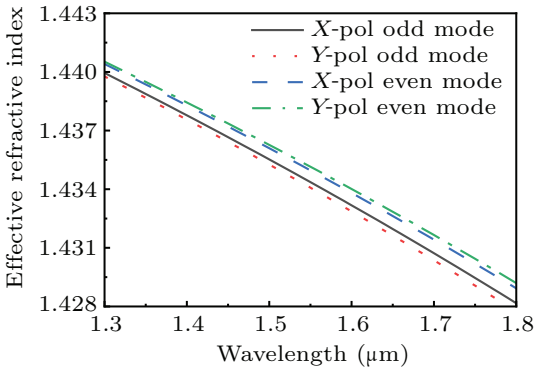


Fig. 2. Effective refractive indices of X-pol odd mode, X-pol even mode, Y-pol odd mode, and Y-pol even mode of the proposed DC-PCF PBS in considered wavelength range from 1.3 μm to 1.8 μm.

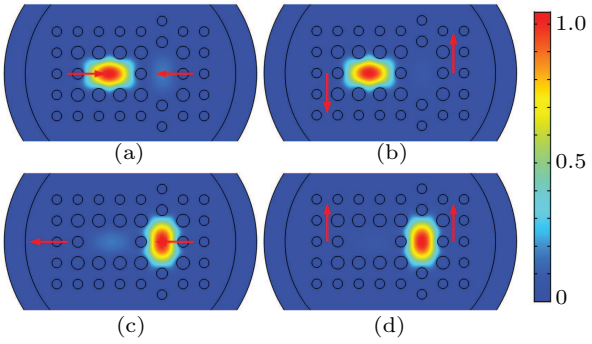


Fig. 3. Mode field distribution of (a) X-pol odd mode, (b) Y-pol odd mode, (c) X-pol even mode, and (d) Y-pol even mode of the proposed DC-PCF PBS calculated at wavelength 1.55 μm, with red arrows representing the directions of electric fields in cores A and B.

Figure 4 shows $CL_{X,Y}$ and CLR of the proposed DC-PCF PBS. Figure 4 demonstrates the decreasing trends of the $CL_{X,Y}$ and the increasing trend of the CLR, which are consistent with the results obtained from Eqs. (2) and (3). The trend that $CL_{X,Y}$ decreases and CLR increases is attributed to the fact that the difference in effective refractive index between the X-pol and Y-pol odd and even modes increase faster as wavelength increases. The CL_X and CL_Y calculated at wavelength 1.3 μm are 1.42 mm and 0.86 mm, respectively, and the corresponding CLR is 1.65. With the increase of wavelength, the CLR at wavelength 1.55 μm is calculated to be 1.79.

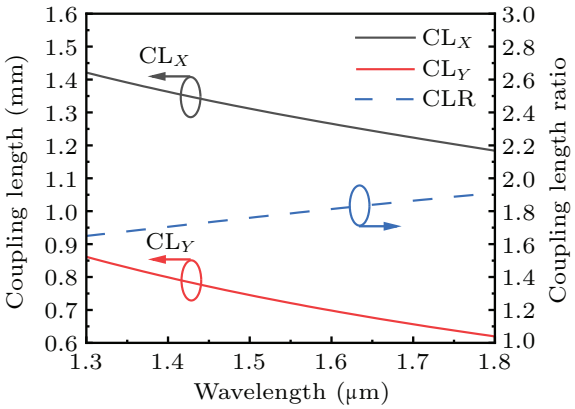


Fig. 4. Variation of CL_X, CL_Y, and CLR of the proposed DC-PCF PBS with wavelength.

In the following, the effects of the structure parameters (d_1, d_2, d_3, and Λ) of the proposed DC-PCF PBS on the CL_X, CL_Y, and CLR will be analyzed in the considered wavelength range from 1.3 μm to 1.8 μm. Figures 5(a)–5(c) show the calculated CL_X, CL_Y, and CLR as functions of wavelength when d_1 changes from 1.8 μm, to 1.9 μm, to 2.0 μm, to 2.1 μm, and to 2.2 μm, respectively. From Figs. 5(a) and 5(b), for different values of d_1, the CL_X and CL_Y curves show the decreasing trends as wavelength increases, and the CL_X value is larger than the CL_Y value at the same d_1. Moreover, at the determined wavelength, the CL_X and CL_Y values decrease as d_1 increases. From Fig. 5(c), the CLR value increases gradually with the increase of wavelength, and decreases with d_1 increasing.

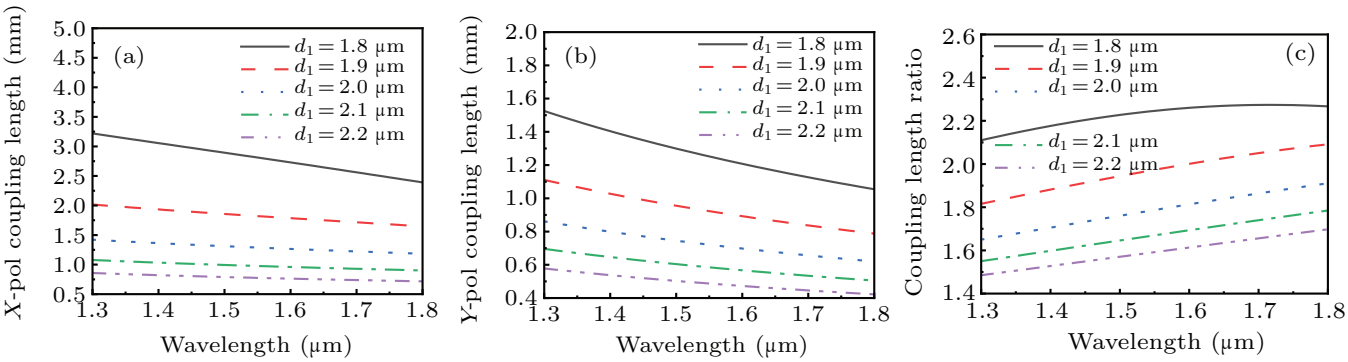


Fig. 5. Effects of d_1 on (a) CL_X, (b) CL_Y, and (c) CLR of the proposed DC-PCF PBS.

When d_2 changes from 1.4 μm, to 1.5 μm, to 1.6 μm, to 1.7 μm, and to 1.8 μm, respectively, the calculated variations of CL_X, CL_Y, and CLR with wavelength are shown in Figs. 6(a)–6(c). From Figs. 6(a) and 6(b), for different values of d_2, the CL_X and CL_Y gradually decrease as wavelength increases, and the CL_X value is larger than the CL_Y value under

the same d_2. At the determined wavelength, the CL_X and CL_Y values increase as d_2 increases. In addition, unlike the scenario of CL_X, the change of the CL_Y curve on the shorter wavelength side is more sensitive than that at the longer wavelength side. From Fig. 6(c), the CLR curves show the increasing trends as wavelength increases, and the CLR value increases with d_2 increasing.

Figures 7(a)–7(c) show the calculated CL_X, CL_Y, and CLR for d_3 changing from 1.3 μm, to 1.4 μm, to 1.5 μm, to 1.6 μm, and to 1.7 μm, respectively. From Figs. 7(a) and 7(b), for different values of d_3, the CL_X value decreases steadily as wavelength increases, and the change of the CL_Y value shows the similar trend to that of the CL_X. Moreover, the CL_X and CL_Y values slightly increase with the increase of d_3 at the determined wavelength. However, comparing with d_1 and d_2, the change of d_3 has the smallest effect on the CL_X and CL_Y curves. From Fig. 7(c) it follows that the CLR curves show the increasing trends, and the CLR values slightly increases with d_3 increasing.

Finally, when Λ changes from 3.0 μm, to 3.1 μm, to 3.2 μm, to 3.3 μm, and to 3.4 μm, respectively, the calculated variations of CL_X, CL_Y, and CLR with wavelength are shown in Figs. 8(a)–8(c). From Figs. 8(a) and 8(b), for different values of Λ, the CL_X and CL_Y decrease as wavelength increases, and the CL_X value is larger than the CL_Y value under the same Λ. The CL_X and CL_Y values increase as Λ increases at the determined wavelength. From Fig. 8(c), the CLR curves show that the increasing trends, and the CLR value decreases as Λ increases. And the change of the CLR curves on the longer wavelength side is more sensitive to the variation of Λ than that on the shorter wavelength side.

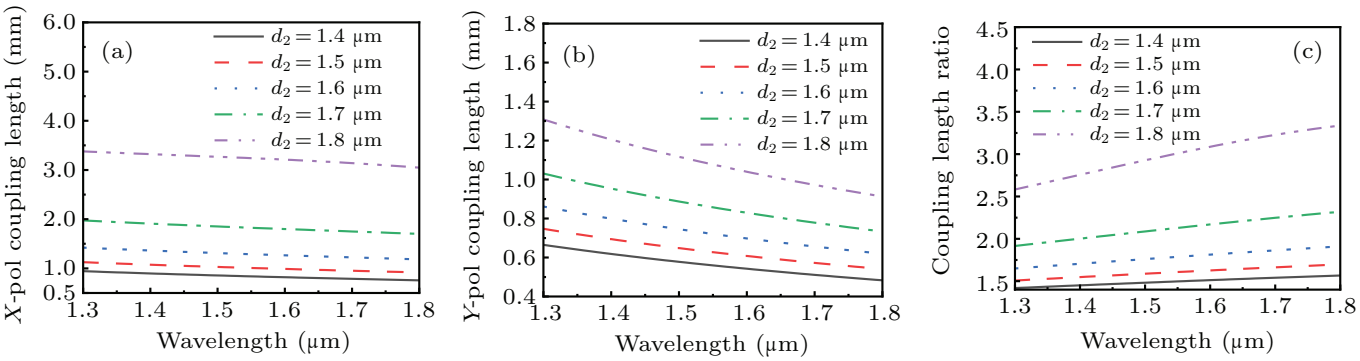


Fig. 6. Effects of d_2 on (a) CL_X, (b) CL_Y, and (c) CLR of the proposed DC-PCF PBS.

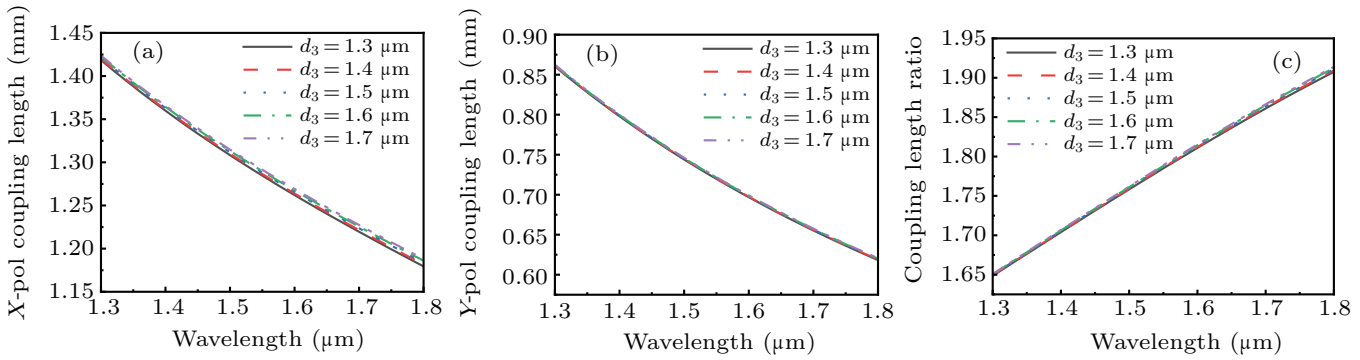


Fig. 7. Effects of d_3 on (a) CL_X, (b) CL_Y, and (c) CLR of the proposed DC-PCF PBS.

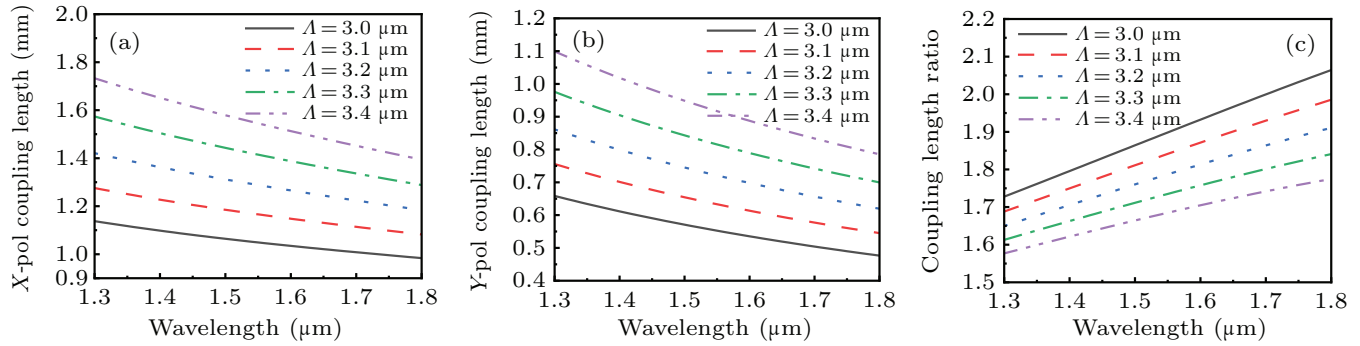


Fig. 8. Effects of Λ on (a) CL_X, (b) CL_Y, and (c) CLR of the proposed DC-PCF PBS.

4. Performances of the proposed DC-PCF PBS

According to the above analyses, we finally choose the optimized structure parameters of the proposed DC-PCF PBS as follows: $d_1 = 2.0$ μm, $d_2 = 1.7$ μm, $d_3 = 1.5$ μm, and $\Lambda = 3.3$ μm. With these parameters, the calculated CL_X, CL_Y, and CLR curves are shown in Fig. 9. From Fig. 9, the CLR value at wavelength 1.55 μm is very close to 2. Next, we will analyze the performances of the proposed DC-PCF PBS, including the splitting length, ER, bandwidth, and IL.

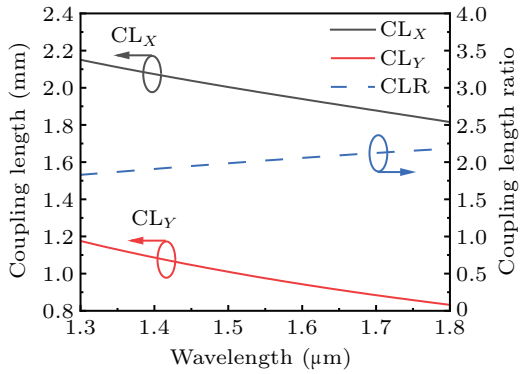


Fig. 9. Calculated variations of CL_X, CL_Y, and CLR of the proposed DC-PCF PBS under optimized structure parameters.

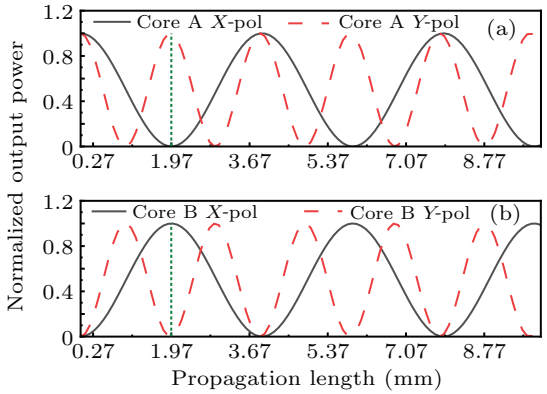


Fig. 10. NOPs of X-pol light and Y-pol light in (a) core A and (b) core B of the proposed DC-PCF PBS on the assumption that the light beam at wavelength 1.55 μm launches into core A.

When the light beam at wavelength 1.55 μm is launched into the core A of the proposed DC-PCF PBS, the calculated NOPs of the X-pol and Y-pol light in the cores A and B are shown in Fig. 10. From Fig. 10 it follows that the X-pol and Y-pol lights have the periodic power exchanges between the two cores. This indicates that the mixed polarized light can be split into two orthogonally polarized light beams at a specific length. Here, the shortest splitting length is 1.97 mm. At the length of 1.97 mm, the NOP of the X-pol light reaches a minimum value while that of the Y-pol light reaches a maximum value in the core A. In contrast, the NOP of the X-pol light reaches a maximum value while that of the Y-pol light reaches a minimum value in the core B. Therefore, the X-pol light and Y-pol light at a wavelength of 1.55 μm are completely separated in the two cores when the splitting length is 1.97 mm.

Figure 11 shows that the ER of the proposed DC-PCF PBS in core A at the shortest splitting length of 1.97 mm, has a sharp downward peak in the wavelength range from 1.3 μm to 1.8 μm, and the extreme value of −81.45 dB appears at wavelength 1.552 μm. Moreover, the bandwidth of the ER less than −20 dB reaches 340 nm (1.38 μm–1.72 μm), which covers the S + C + L + U communication bands.

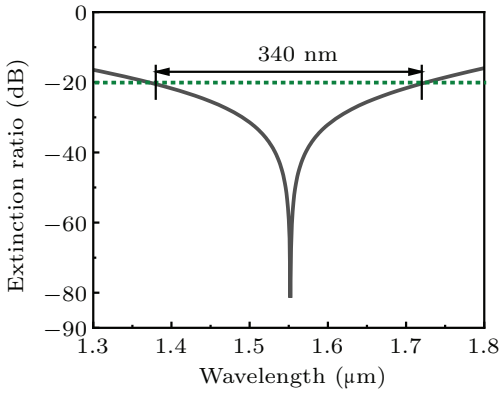


Fig. 11. Variation of ER with wavelength of the proposed DC-PCF PBS for splitting length of 1.97 mm.

The comparisons between the proposed DC-PCF PBS and other reported structures are shown in Table 1. It can be seen from Table 1 that the proposed DC-PCF PBS has the largest bandwidth and highest ER. Although the PBSs in Refs. [19,38] have the shorter splitting lengths, their structures are more complex. Therefore, the proposed DC-PCF PBS has simple structure and good performances, and is possible to be fabricated in practice.

Table 1. Comparations between the proposed DC-PCF PBS and other reported structures.

Refs.	Types of air holes	Number of air holes	Bandwidth (nm)	Max ER (dB)	Splitting length (mm)
[19]	Two kinds of circular holes and three kinds of elliptic holes	114	48 (1526–1574)	–42.9	0.254
[38]	One kind of circular holes and one kind of elliptic holes	68	70 (near 1550)	–79.3	0.0933
[39]	Two kinds of elliptic holes	59	100 (near 1500)	–52.5	2
[40]	Four kinds of circular holes	76	116 (1481–1597)	–31	5.9
This work	Three kinds of circular holes	37	340 (1380–1720)	–81.45	1.97

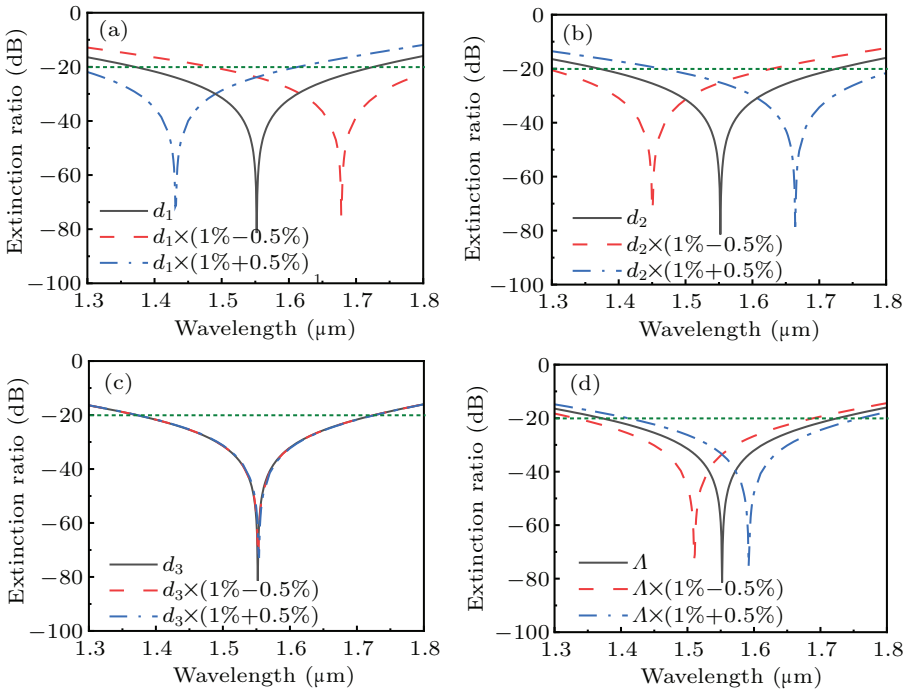


Fig. 12. Variations of the ER under the fabrication error 0.5% for (a) d_1, (b) d_2, (c) d_3, and (d) Λ.

The fabrication tolerance of the structure parameters of the proposed DC-PCF PBS is important in practical applications. Figures 12(a)–12(d) show the changes of the ER under a fabrication error of 0.5% for different structure parameters. From Figs. 12(a), 12(b), and 12(d), when d_1, d_2, and Λ are changed by $\pm$0.5%, the working bandwidth of the DC-PCF PBS will be blue-shifted or red-shifted, but they can still maintain above 300 nm. And the ER at wavelength 1.55 μm is kept below −20 dB. From Fig. 12(c), the working bandwidth and ER of the proposed DC-PCF PBS are hardly affected when d_3 changes.

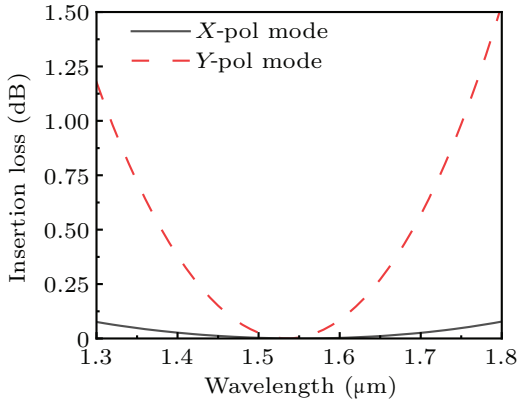


Fig. 13. Valuation of IL of X-pol light and Y-pol light with wavelength in the wavelength range from 1.3 μm to 1.8 μm.

For the proposed DC-PCF PBS, the IL is also investigated by Eq. (7), and the results are shown in Fig. 13. From Fig. 13, the ILs of the X-pol light and Y-pol light first decrease and then increase. In the wavelength range from 1.3 μm to 1.8 μm, the IL of the X-pol light is lower than that of the Y-pol light, and the two beams reach a minimum value at wavelength 1.55 μm, where the IL of the X-pol light and Y-pol light are 5.35×10^{-6} dB and 4.20×10^{-3} dB, respectively.

5. Conclusions

In summary, a novel DC-PCF PBS with two kinds of lattices and three kinds of air holes is proposed. The FV-FEM and dual-core coupled mode theory are used to analyze the propagation characteristics. The simulation results show that the bandwidth of the proposed DC-PCF PBS reaches to 340 nm, which covers the S + C + L + U communication bands, and the splitting length is 1.97 mm. Moreover, the maximum ER at wavelength 1.552 μm is −81.45 dB, and the ER at wavelength 1.55 μm is −59.08 dB. Finally, the calculated IL of the X-pol light and Y-pol light are 5.35×10^{-6} dB and 4.20×10^{-3} dB, respectively. The proposed DC-PCF PBS has the simple structure, ultra-wide bandwidth, high ER, and low IL. It has important applications in the field of all-optical communication and network.

Acknowledgement

Project supported by the National Key Research and Development Project of China (Grant No. 2019YFB2204001).

References

[1] Fang L and Wang J 2018 *Opt. Express* **26** 15124
[2] Yu W, Yao P, Wang P and Ming H 2013 *Optik* **124** 5489
[3] Sun Y, Zhang L, Xia H, Cao S, Wang L, Yang S, Wu Y and Tai R 2021 *Optik* **227** 166096
[4] Dai H, Shang J and Chen X 2017 *Opt. Eng.* **56** 077107
[5] Tang X, Liao J, Li H and Liu Y 2013 *IEEE J. Quantum Electron.* **49** 43
[6] Li Y, Deng J, Yang Z, Zou H and Ma Y 2022 *Chin. Phys. B* **31** 054215

[7] Tajima K, Zhou J, Nakajima K and Sato K 2004 *Journal of Lightwave Technology* **22** 7
[8] Selvendran S, Divya J, Raja A S, Sivasubramanian A and Itapu S 2022 *Micromachines* **13** 917
[9] Zheng Y Q, Liu J Q, Wang Y F, Liu H, Wang W and Xie X P 2022 *Microwave and Optical Technology Letters* **65** 1277
[10] Knight J C 2003 *Nature* **424** 847
[11] Russell P 2003 *Science* **299** 358
[12] Bing P, Wu G, Liu Q, Li Z, Tan L, Zhang H and Yao J 2022 *Chin. Phys. B* **31** 084208
[13] Huang Y, Yang H and Mao Y 2022 *Chin. Phys. B* **31** 054211
[14] Zheng W, Ma Z, Kang L, Zhang M and Liu C 2022 *Optik* **271** 170089
[15] Zou H, Xiong H, Zhang Y S, Ma Y and Zheng J J 2017 *Chin. Phys. B* **26** 124216
[16] Zi J, Li S, An G and Fan Z 2016 *Opt. Commun.* **363** 80
[17] Chu L, Liu M, Shum P and Fu Y 2019 *Appl. Opt.* **58** 7892
[18] Zhang X, Liu Z, Gui Y, Gan H, Guan Y, He L, Wang X, Shen X and Dai S 2021 *Opt. Express* **29** 39601
[19] Ren C, Yuan J, Wang K, Yan B, Sang X and Yu C 2021 *Opt. Eng.* **60** 017102
[20] Zhang J X 2022 *J. Nanophoton.* **16** 016005
[21] Zhao X T, Hua L, Xiong Q, Jiang G H and Cheng J R 2019 *Opt. Quantum Electron.* **51** 162
[22] Zhang Y, Qu Y, Yuan J, Wang H, Zhou X, Huo J, Yan B, Wu Q, Wang K, Long K and Yu C 2021 *Fiber and Integrated Optics* **40** 70
[23] Qu Y, Yuan J, Wang K, Qiu S, Zhou X, Yan B, Wu Q, Liu B, Wang K, Sang X, Long K and Yu C 2022 *J. Opt. Soc. Am. B* **39** 1580
[24] Tong H T, Koumura A, Nakatani A, Nguyen H P T, Matsumoto M, Sakai G, Suzuki T and Ohishi Y 2022 *Opt. Express* **30** 25433
[25] Mahfuz M A, Mollah Md A, Momota M R, Paul A K, Masud A, Akter S and Hasan Md R 2019 *Opt. Mater.* **90** 315
[26] Tao Y, Ye H, Ding Y, Ren X and Liu X 2022 *Photonic Sens* **12** 220309
[27] Malitson I H 1965 *J. Opt. Soc. Am.* **55** 1205
[28] Di Bin P and Mothe N 2009 *Opt. Express* **17** 15778
[29] Liu E, Liang S and Liu J 2019 *Superlattices and Microstructures* **130** 61
[30] Zou H, Xiong H, Zhang Y S, Ma Y and Zheng J J 2017 *Chin. Phys. B* **26** 124216
[31] Qu Y, Yuan J, Qiu S, Zhou X, Li F, Yan B, Wu Q, Wang K, Sang X, Long K and Yu C 2021 *Sensors* **21** 496
[32] Rahman M T and Khaleque A 2019 *Appl. Opt.* **58** 9426
[33] Qu Y, Han Y, Yuan J, Zhou X, Yan B, Wang K, Sang X and Yu C 2021 *Photonics* **8** 461
[34] Zou H, Xiong H, Zhang Y S, Ma Y and Zheng J J 2017 *Chin. Phys. B* **26** 124216
[35] Zhao T, Lou S, Wang X, Zhou M and Lian Z 2016 *Appl. Opt.* **55** 6428
[36] He Y, Zhang Y, Zhang R, Sun L and Su Y 2021 *Opt. Lett.* **46** 194
[37] Dou C, Jing X, Li S, Wu J and Wang Q 2018 *Opt. Quantum Electron* **50** 255
[38] Wang H, Yan X, Li S, An G and Zhang X 2017 *J. Mod. Opt.* **64** 445
[39] Rajeswari D, Sivanantha Raja A and Selvendran S 2017 *Optik* **144** 15
[40] Chen M Y, Sun B, Zhang Y K and Fu X X 2010 *Appl. Opt.* **49** 3042